The Electron in Zero Theory

Four Layer Field Geometry Maxwell Dynamics Observer Charge Readout Helical Half Action and Literature Input Output Audit

S. M. H. Emamifar

Research manuscript version 2.2 · 17 September 2026

ORCID: 0009-0007-6257-0163

Abstract

Zero Theory describes the electron as a complete, wound, two-wave electromagnetic field organized into four coupled phase sectors. Within the declared model, the observer-facing L1 shell and its hidden symmetric L4 partner obey a half-angle relative-frame law: a 720-degree L1 phase advance is required for recurrence of the oriented, layer-labeled state, whereas an unoriented control returns after 360 degrees. The corrected L1 construction combines azimuthal circulation with an externally attached axial mode to form a 45-degree helix. Although the oscillating field has zero linear phase average, its quadratic Poynting flux retains one propagation direction. For the attached helical mode, the one-turn clock gives omega-turn = c/(sqrt(2)R), while its angular momentum per attached energy is Jz/Uattached = R/(sqrt(2)c). Their product is exactly one half, independent of radius, propagation speed, and field amplitude. If one quantum of that same mode obeys Uattached = hbar times omega-turn, the conditional result is Jz = hbar/2. This result is derived without legacy prescribed-source transport rates; those settings belong to a separate historical field diagnostic and are not part of the present spin inference. The manuscript also states a limited observer-charge mechanism: when the electric and magnetic directions are phase-locked to the bound layer geometry, an external observer can read a persistent outward electric projection as charge-like response. No Coulomb-field magnitude, elementary charge, or g factor is inferred from that statement. A source-checked input-output audit prevents fitted recovery of electron observables from being mistaken for an independent prediction.

Keywords: electron; Zero Theory; four-layer field geometry; Maxwell simulation; L1 observer; L1-L4 frame slip; blind field-frame readout; 4-pi recurrence; helical flux; angular momentum.

1 The electron as a foundational field structure

An account of electron geometry must explain what carries the structure, what keeps it coherent, and what an experiment would measure. A toroidal drawing answers only part of the first question. A useful model must also say whether its curves represent charge trajectories, field lines, phase contours or energy-flow paths; these objects can have different motion and different observable consequences. Zero Theory approaches the electron through an organized, recurrent field rather than through a rigid material ring. Its four layers describe the internal organization of a complete wound field and provide the starting point for the electromagnetic and observer-response calculations developed below. [Z1–Z3]

The central construction begins with two seed waves and two mirror-related branches. Each branch has an anchor sector and an active sector, producing four phase sectors in total. Their continuous capacities, phase recurrence and paired electromagnetic roles are specified within the model. This gives the proposal more content than a single torus ansatz: the theory must preserve the relationships among all four sectors whenever it assigns a current, an energy or an observer-dependent rate. It also places a burden on the eventual field equations. A local relation that works for one sector must remain consistent with the complete knot and with the common observer used to compare sectors.

Three levels of statement recur throughout this paper. A **model premise** specifies the proposed physical organization, such as the radial electric–magnetic partition. A **conditional result** follows from declared premises, such as the minimum admissible recurrence count. A **numerical diagnostic** establishes a property of a specified computational problem, such as preservation of a Maxwell constraint. An experimental conclusion requires an additional correspondence between the model variable and the measured quantity. These distinctions allow the electron programme to accumulate results without turning a successful arithmetic identity or solver check into a claim about an uncomputed laboratory observable.

The four-layer formation and recurrence mechanism is treated here as the established conditional architecture of the manuscript. A first-principles evolution equation for the complete interacting field would deepen that architecture. It is a distinct task from explaining or recovering the architecture already specified. In particular, the existence of a remaining quantitative transfer law does not erase the geometric mechanism that motivates it. [Z1, Z4]

2 What the four layers represent

2.1 One field with four phase sectors

Let $\Phi_w(x,t)$ describe a phase coordinate of the wound field. A sector can be represented as the region in which that phase lies in a designated interval I_i:

$$L_i(t)=\{x:\Phi_w(x,t)\in I_i\},i=1,2,3,4.$$

Its boundary is a phase level set $\Sigma_{i,a}(t)=\{x:\Phi_w=\phi_{i,a}\}$. Where the phase is differentiable and its gradient is nonzero, the normal velocity of that level set follows by differentiation:

$$v_n=-\frac{\partial_t\Phi_w}{|\nabla\Phi_w|}.$$

This equation describes the motion of a phase boundary. It does not assign the same velocity to matter, charge, a fluid element or energy transport. It also does not give an independent equation of motion for each layer. All four sectors belong to the same complete field. Treating them as four independently chosen material membranes would introduce degrees of freedom that the stated ontology does not grant. [Z1]

Two different pairings must be retained. The branch genealogy groups $(L1,L2)$ and $(L4,L3)$: each seed branch supplies an anchor and an active sector. The electromagnetic mirror pairing groups $L1\leftrightarrow L4$ and $L2\leftrightarrow L3$. Genealogy answers where a sector belongs in the construction; electromagnetic pairing answers which sector participates in its corresponding mirror relation. Figure 1 separates these roles.

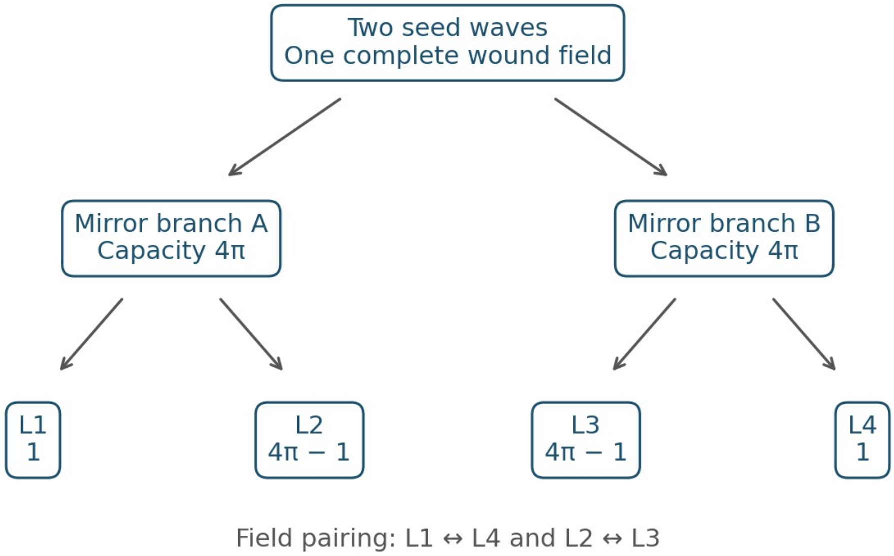

Figure 1. Sector genealogy and field pairing. The diagram represents relationships, not a Euclidean embedding or four independent material rings. Numbers beneath the layer labels are continuous capacities.

2.2 Capacity is a typed quantity

The assigned capacity vector is

$$(C_1, C_2, C_3, C_4) = (1, 4\pi - 1, 4\pi - 1, 1).$$

Each branch has capacity 4π, and the complete construction has capacity 8π. The outer anchors have unit capacity, while each inner active sector carries the remaining $4\pi - 1$. These are continuous model capacities. They are not automatically counts of photons, injection events, crests, spatial windings or elapsed ticks. A conversion among these quantities needs its own rule. [Z1]

This distinction becomes essential when the same construction produces a six-cycle recurrence and a separate construction count of 2830. Those numbers answer different questions. Six is selected by a terminal saturation rule; 2830 follows from a declared injection and closure prescription. Neither number is the total continuous capacity 8π expressed in another notation.

2.3 Side clipping and winding sense

The seed interaction is described as an offset, or side-clipping, encounter. Such an encounter can have zero net linear momentum while retaining angular momentum. For example, take two equal and opposite momenta in a plane:

$$r_1 = (0, b/2, 0),\ p_1 = (p, 0, 0),\ r_2 = (0, -b/2, 0),\ p_2 = (-p, 0, 0).$$

Then $P = 0$ while $L_z = -b\,p$. The calculation establishes the kinematic possibility of a circulating remnant from an offset encounter. It does not determine the electron's angular momentum or prove that the remnant is stable.

Wave-flow direction and winding chirality are separately owned variables. Reversing a traversal and applying a mirror transformation can compensate in their effect on a winding sign. Consequently, a diagram of counter-propagating seeds need not describe opposite final winding chirality. Conversely, an unlabeled seed pair that is invariant under a half-turn does not thereby acquire a physically observable 720-degree spinor recurrence. The model's own mirror controls preserve this distinction. [Z3]

3 Saturation and the six-cycle recurrence

3.1 Selection of the minimum admissible integer

In the wounded, co-rotating construction, capture and redshift are proposed to compress active content until a minimum admissible wavelength or saturation limit is reached. A reduced feedback description connects compression, overlap and capture. Its mobilities and couplings are phenomenological; they should not be read as coefficients already derived from a complete Maxwell action. The recurrence selection uses a more specific capacity rule. [Z1, Z2]

Write $C=4\pi-1$. For a candidate integer recurrence count N, define the model's compression readout and its associated parameter by

$$S_N=\frac{C}{N},\beta_N=S_N-1.$$

Under the declared admissibility condition $0\le\beta_N<1$, the allowed integers satisfy

$$\frac{C}{2}<N\le C.$$

Since $C=11.566370614\ldots$, the allowed set is $N\in\{6,7,8,9,10,11\}$. The saturation rule selects the greatest admissible compression, hence the smallest admissible integer:

$$N_{terminal}=6,\beta_6=0.9277284357265288\ldots.$$

The rejected $N=5$ candidate gives $\beta_5=1.3132741228718346\ldots$. Thus the six-cycle result is exact under two ingredients: the stated capacity-to-readout law and the rule choosing maximal admissible compression. The inequality alone leaves six allowed integers and does not uniquely select six. Nor does the calculation independently establish that β_N is a particular laboratory velocity ratio. That interpretation belongs to the frame and readout map. [Z2]

3.2 Equal phase cells and their symmetry

For six equal consecutive cells on a uniform phase coordinate α, a representative phase law is

$$\Phi(\alpha)=6\alpha+\Phi_0,\alpha_k=\alpha_0+\frac{2\pi k}{6},k=0,\ldots,5.$$

The spacing is $\pi/3$ and the six points form three antipodal pairs. The converse is false: three arbitrary antipodal pairs need not have equal spacings. Equal-cell closure supplies the extra restriction. Figure 2B illustrates the phase recurrence using a cosine; that illustrative waveform is not a recovered full-field solution.

The recurrence of $\exp(i6\alpha)$ under $\alpha\mapsto\alpha+\pi/3$ is a statement about the chosen phase coordinate. It becomes a 60-degree spatial rotation only if the mapping from that coordinate to spatial orientation is uniform and specified. Similarly, six phase cells do not by themselves fix a three-dimensional torus-knot class, a Hopf invariant or a quantum angular-momentum representation. Those assignments require their own field or configuration-space definitions. [Z2]

3.3 What restores a disturbed phase pattern

A common angular rotation preserves phase errors rather than healing them. A naive all-to-all synchronization rule can also be counterproductive: it tends to cluster crests instead of retaining six separated cells. The reduced stiffness construction therefore preserves total winding while allowing local phase-gradient errors to relax. For a periodic perturbation $\delta(\alpha,t)$, its illustrative diffusion equation is

$$\partial_t \delta = D \partial_\alpha^2 \delta , D > 0 .$$

For Fourier modes δ_n, the solution is $\delta_n(t) = \delta_n(0) e^{-Dn^2 t}$. Nonuniform modes decay; the global phase offset remains neutral. The archived reduced tests include disturbed mirror phases, with random offsets of order ten degrees. They support the stated restoring mechanism within that reduced model. They do not determine D from the complete field or prove stability against all radial, radiative and topological perturbations. The result identifies what kind of restoring law is needed and rules out two inadequate substitutes. [Z2]

4 Local cross section and paired electromagnetic evolution

4.1 The corrected local geometry

For the declared L1 local-observer construction, the inner boundary is at zero radius and the midline lies halfway to the outer boundary:

$$R_{in} = 0 , R_{mid} = \frac{R_{out}}{2} , d_1 = R_{out} .$$

Thus $C_{out} = 2 C_{mid}$. These relations define this local geometry. A change of observer or normalization requires an explicit translation before the same symbol is used for a laboratory radius. In particular, a dimensionless radius in a computational candidate is not automatically this local radius or an experimentally constrained charge radius. [Z3, Z7]

The specified electromagnetic cross section allocates the outer three quarters of the radial thickness to the electric sector and the inner quarter to the magnetic sector:

$$d_E = 0.75 d_1 , d_B = 0.25 d_1 , R_{EB} = 0.25 R_{out} .$$

In the declared L1 face description, the outer sector is electric-only and the inner sector magnetic-only. This is a physical radial allocation within the model, not merely a color convention in a drawing. It is also a premise. The stationary electromagnetic-energy test recorded in the earlier v0.3 work did not independently select the interface fraction $q = 0.25$. That negative result remains relevant. [Z3, Z4]

A thickness ratio cannot be substituted for an area ratio, energy fraction or detector weight. Energy depends on the field profile and the integration measure. Even for a circular cross section, changing a radial interface changes area quadratically; changing energy additionally depends on E^2 and B^2. The 75/25 allocation therefore cannot be inferred from a convenient 1:3 area arithmetic or from the support inequality in Section 5.

4.2 The Maxwell subsystem is a pair

The corresponding face-attached mapped components of the outer sectors obey

$$E_4 = - E_1 , B_4 = + B_1 , J_4 = - J_1 .$$

The complete outer electromagnetic cycle is assigned to $L1 + L4$. L1 alone is not the complete Maxwell subsystem. The earlier interpretation of an isolated L1 free-wave sinusoid is superseded. Here “frozen” means that sector identity and orientation remain attached to the layer geometry; it does not mean that the electromagnetic field is static for every observer. Moving geometry changes the common-observer field decomposition. [Z3, Z4]

These are mapped-basis relations. One cannot simply add the displayed components as if they were already evaluated at the same spacetime event in the same basis and conclude that an observable electric field vanishes. The spatial map, temporal synchronization and basis transformation must first be supplied. This requirement matters whenever the model passes from its internal symmetry description to a common Maxwell field.

The scalar frame-slip prescription is

$$\Delta\Theta_{14}=1/2\,\Delta\theta_{EM,14},\Delta\Theta_{23}=1/2\,\Delta\theta_{EM,23}.$$

The physical owner of this scalar law is the induction-driven slip of the oriented frame between each symmetric pair: every 180-degree electromagnetic advance produces 90 degrees of relative frame slip. For either pair define the complete labeled scalar state

$$\mathcal{K}(\theta) = \left(\theta \ mod \ 2\pi, \frac{\theta}{2} mod \ 2\pi\right)$$

Because the second component retains an oriented, layer-labeled frame rather than an unoriented axis,

$$\mathcal{K}(2\pi) = (0,\ \pi) \neq \mathcal{K}(0), \qquad \mathcal{K}(4\pi) = (0,\ 0) = \mathcal{K}(0)$$

The executable v0.11 audit verifies this relation exactly for both L1-L4 and L2-L3. The first positive return is therefore 4-pi, or 720 degrees. Its negative control replaces the oriented frame by an unlabeled axis with period pi; that control returns after 2-pi. Thus the 4-pi result depends on preserving orientation and layer identity and is not generated by the half-angle arithmetic alone.

This closes the labeled scalar recurrence map. It still does not select a unique three-dimensional rotation axis, furnish a complete SO(3) material-frame history, define a deformation torque, or determine the magnitude of angular momentum. Those are separate dynamical and observational calculations.

4.3 The middle-pair cancellation control

The middle-pair local control uses E_2 along $+y$, B_2 along $+z$ and J_2 along $+x$, together with the mirror/reverse signs $E_3=-E_2$, $B_3=+B_2$ and $J_3=-J_2$. Within its force-free local assumptions, the self and cross force terms cancel. Changing only a branch amplitude or adding only a phase lag does not supply the constitutive asymmetry needed to evade that cancellation. [Z3]

This is a useful negative result. It prevents an attractive-force claim from being obtained by selectively keeping one Lorentz-force term while discarding its paired counterpart. It is not a universal theorem excluding every finite-width four-sector solution. A proposed escape must identify which field/source relation changes and demonstrate that the complete force balance changes with it.

5 Curvature support asymmetry and field capture

5.1 Why bending changes the support comparison

The formation mechanism links bending of a propagating field to transfer into mirror-ring channels. In the straight-path comparison, transverse support is available on both sides. For a circular path of radius R, the inward normal direction reaches the center after distance R, while the outward direction has no corresponding curvature-center cutoff. The mathematical comparison must therefore retain the outward tail. Replacing that tail by a second finite disk changes the problem. [Z4]

Let $s \geq 0$ be transverse distance from the midline, and let $u(s) \geq 0$ be a common localized support profile. In the planar circular-band formalization,

$$U_{in}=2\pi\int_0^R u(s)(R-s)\,ds,U_{out}=2\pi\int_0^\infty u(s)(R+s)\,ds.$$

Subtracting gives

$$\Delta U_{support} = 4\pi \int_0^R s\,u(s)\,ds + 2\pi \int_R^\infty (R+s)\,u(s)\,ds > 0.$$

Strict positivity requires a nonzero contribution at positive s on a set of nonzero measure; a profile concentrated only at the midline does not establish the strict inequality. The integrals must converge. An unbounded support domain is therefore compatible with finite integrated content.

The comparison proves an integrated geometric inequality under the common-profile assumption. It does not require the pointwise electric intensity at equal inward and outward distances to differ. It also does not yet supply the actual self-consistent field profile. The factors $2\pi(R \pm s)\,ds$ are planar band areas: for U to denote energy, u must carry the corresponding energy-per-area units, possibly after integrating another direction. Substitution of a three-dimensional volume energy density without that reduction would be dimensionally incorrect.

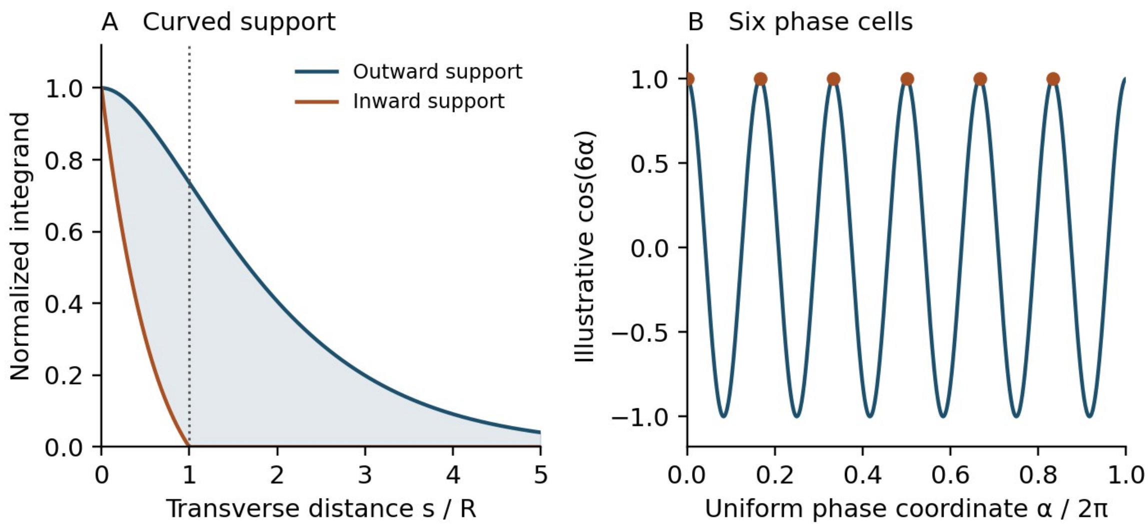

Figure 2. Conditional geometric illustrations. A uses the illustrative profile u(s) proportional to exp(−s/R); the inward contribution ends at s/R = 1 and the outward tail continues. B displays six equal cells on a uniform phase coordinate. Neither panel is a three-dimensional Maxwell solution or a fitted electron field.

5.2 Where the attenuated content goes

The proposed receiving channel is part of the electron architecture. Unmatched propagating content transfers into the symmetric rings, rather than disappearing. For the outer pair, the stated induction association is

$$E_{L1,outer}^{75\%} \leftrightarrow B_{L4,outer}^{75\%},$$

with the reciprocal association and corresponding middle-pair organization. This names complementary receiving sectors. It answers a different question from the component parity relations in Section 4.2; both must eventually be implemented in a common field description. [Z4]

The mechanism is consequently specific: closed curvature produces asymmetric transverse support; the unmatched contribution is assigned to mirror-sector induction; the freely propagating channel attenuates while stored knot content increases. Attenuation refers to one channel. Total energy conservation requires including the receiving field, any source work and any outgoing flux.

A quantitative capture prediction additionally needs a cycle-by-cycle transfer rule, a physical profile and a normalization. The positive support difference alone gives neither a damping coefficient nor the number of encounters required for closure. The construction count in Appendix A is obtained from a separate injection prescription and must not be silently identified with a damping time inferred from this integral. A microscopic transfer equation connecting these constructions would be a substantive further result.

6 Charge sources and the energy of the complete knot

6.1 A mirror-compatible source family

One registered source family distributes a normalized total charge Q_* between the outer and middle sectors:

$$\left(Q_1, Q_2, Q_3, Q_4\right)=\frac{Q_*}{2}\left(a_Q, 1-a_Q, 1-a_Q, a_Q\right), 0 \le a_Q \le 1 .$$

Here a_Q is an allocation parameter, not the fine-structure constant or a phase angle. The sectors have equal charge within each mirror pair, $Q_4=Q_1$ and $Q_3=Q_2$, while their mapped currents can reverse. Additional parameters allocate charge among interfaces and boundary sheets. Setting $Q_*=1$ normalizes this family; it does not derive the magnitude or SI sign of electron charge. [Z5]

A nonzero net charge can produce a far-field monopole through Gauss's law. That leading behavior alone does not select the internal toroidal structure: many localized source distributions share the same total charge. Finite-distance multipoles and scattering form factors depend on the spatial and temporal source profile. The internal geometry becomes experimentally discriminating only when it fixes these further responses without choosing them to reproduce the desired measurement.

6.2 Cross terms belong to the electron

The complete electromagnetic field is assembled before its energy and momentum are evaluated. With F_i denoting the sector contributions represented in a common frame,

$$F_{knot}=\sum_i F_i, T_{EM}^{\mu\nu}\left(F_{knot}\right) \neq \sum_i T_{EM}^{\mu\nu}\left(F_i\right)$$

in general. The stress-energy tensor is quadratic in the field. For example, its electric energy contains both the individual $|E_i|^2$ terms and the interference terms $2 E_i \cdot E_j$. Ignoring the latter changes the model's energy, stress and force balance. [Z5]

With the convention $x^0=c t$, the electromagnetic contribution to four-momentum can be written

$$P_{EM}^{\mu}=\frac{1}{c}\int T_{EM}^{0\mu} d^3 x, Q=\int \rho_{knot} d^3 x .$$

If non-electromagnetic stresses or source degrees of freedom are required, their energy and momentum must also enter the conserved total. The model cannot identify the isolated L1 electric energy with $m_e c^2$ while assigning the balancing sectors no role. A full-field calculation and a declared observer projection are prerequisites for such an identification.

For ordinary Maxwell fields, Poynting's theorem provides the accounting relation

$$\frac{d U_{EM}}{d t}+\oint S \cdot d A=-\int J \cdot E d^3 x .$$

In a prescribed-source calculation, the right-hand side includes exchange with the imposed source motion. Accurate accounting of that exchange is a numerical achievement, but it does not prove that the source trajectory maintains itself without external work. This distinction governs the interpretation of the G1 experiment.

6.3 Operational charge and the dark two-way-road analogy

The model must distinguish an internal layer label from an operational electric charge. A useful analogy is a dark two-way road on which only the lamps are visible. An observer can classify two opposite traffic responses from the motion and effect of the lights, even without seeing the road, the engines, or the hidden mechanism that keeps each vehicle moving. In the same way, the sign of charge is defined operationally by the direction of a system's response to an external electromagnetic probe; it is not established merely by naming an unseen layer electric or magnetic.

For the proposed electron and positron, the mirror role reversal can supply two opposite internal response channels. To promote those channels to negative and positive laboratory charge, however, the theory must specify the same external coupling experiment for both states and recover equal-magnitude, opposite-sign responses. The analogy clarifies what is observed and what remains hidden; it does not derive the elementary charge magnitude e, the Coulomb unit, or the complete charge-current density.

This separation matters for the present work. The 45-degree helix, the half-angle L1-L4 frame law, the 4-pi recurrence, and the clean same-mode action ratio can be tested without first settling the full ontology of electric charge. Charge becomes mandatory when the model is asked to predict the strength and radial form of the external electric field, the elementary charge in SI units, or the response to an external probe.

6.4 Frozen layer vectors and observer-facing charge appearance

In a freely propagating electromagnetic wave, the electric and magnetic vectors evolve together as parts of one traveling field. The bound four-layer proposal adds a distinct model condition: the directions of the local electric and magnetic vectors become phase-locked to their respective layer geometries. Here frozen does not mean that the field vanishes or that time stops. It means that the relative orientation carried by a layer remains attached to the recurring knot instead of passing the observer as an unconstrained traveling phase.

An external observer does not resolve every internal layer separately. The observer receives the boundary projection that survives the ordered L4-to-L1 readout. Internally returning or magnetically counter-directed contributions can remain hidden in the closed structure, while a persistent outward electric-facing component reaches the observation channel. The observer can therefore classify the knot by a stable electric sign and response even though the underlying object is a coupled electromagnetic structure rather than a bare scalar charge.

Qobs(struct) = Pout[sum from a=1 to 4 of wa Ea(locked)]

This expression is a bookkeeping definition of the observer-facing electric projection. The weights wa and the projection Pout belong to the declared layer-readout map; they are not Coulomb units. Reversing the wound orientation can reverse the sign of the projection, providing the candidate distinction between electron-like and positron-like readouts while leaving the internal capacity closure intact.

Claim boundary. This section explains how charge can appear as an observer readout of a frozen, oriented layer structure. It does not derive the elementary charge e, a 1/r-squared Coulomb field, Gauss-law normalization, charge density in SI units, or the electron g factor. Those require a separate external-field and probe-coupling calculation. The qualitative appearance mechanism may therefore be stated without making those later calibrations prerequisites for the spin calculation.

7 The G1 Dynamic Maxwell calculation

7.1 The computational problem

The G1 v0.4 branch evolves Maxwell fields for a declared moving four-layer source candidate. Its laboratory geometry is fixed as the input candidate, while the source assembly follows a prescribed orientation history. The generator uses a dimensionless centerline radius of 0.57, cross-section outer scale 0.34, interface fraction 0.25 and source center $(0, 0.78, 0)$. These are the candidate's computational coordinates. They are not a direct measurement of the local geometry defined in Section 4. [Z6]

The historical G1 calculation uses prescribed source-sheet transport parameters and declared driving constants. Those settings belong only to that prescribed-source Maxwell diagnostic; they are neither electron observables nor inputs to the clean helical half-action result.

$$\Gamma = 63.474324474871096\,, B_0 = 0.002\, s_B\,, B_1 = 0.0001\, s_B\,,$$

with pulse duration $T = \pi / (\Gamma B_1)$. For pulse fraction $f = t / T$, the intended axis path is

$$n(f) = R_z(-20\pi f)\, R_{-\hat{x}}(\pi f)\, \hat{z}\,.$$

It starts at $+\hat{z}$ and ends at $-\hat{z}$. Minimal-twist frames carry the marker geometry along that path. The gyromagnetic coefficient and the path are inputs to this diagnostic. Successful following of that path cannot therefore be reported as an independent prediction of electron precession or of the measured g factor.

The accepted weak driving scale is $s_B = 0.03$. The $s_B = 1$ branch is retained as a stronger stress control. The grid uses a periodic cube of side L and N^3 points, with M source intervals during the pulse. The field update is written in normalized units with unit wave speed. Conversion of a physical clock to these units is addressed in Section 8; the source parameters should not be retrospectively relabeled as native electron phase frequencies.

7.2 Real fields and finite-step continuity

In the normalized field variables, the evolution and constraints have the familiar form

$$\partial_\tau E = \nabla \times B - J\,, \partial_\tau B = -\nabla \times E\,,$$

$\nabla \cdot E = \rho\,, \nabla \cdot B = 0\,, \partial_\tau \rho + \nabla \cdot J = 0\,.$

The source normalization absorbs the electromagnetic constants. The charge and current histories enter these equations through the marker construction; the solver supplies their electromagnetic response. A self-consistent particle calculation would additionally evolve the source degrees of freedom from their interaction with that response.

The earlier v0.3 dynamic representation encountered an even-grid Nyquist/Hermitian consistency problem and a source-time quadrature problem. The v0.4 repair removes exact Nyquist planes on even grids before constructing the dynamic source. This is a numerical representation choice, not a proposed physical filter in the electron. The archive's removed-power diagnostic is at most approximately 7.94×10^{-8}. [Z6]

For each nonzero Fourier wavevector k, the raw current is decomposed into transverse and longitudinal parts. The transverse source is retained, while the longitudinal source is constructed from the charge density at the interval endpoints:

$$\hat{J}_L = \frac{i k}{|k|^2} \frac{\hat{\rho}_{n+1} - \hat{\rho}_n}{h}\,.$$

Consequently,

$$\frac{\hat{\rho}_{n+1} - \hat{\rho}_n}{h} + i k \cdot \hat{J} = 0$$

to floating-point accuracy for the represented nonzero modes. This construction enforces discrete continuity; it is not an independent derivation of the uncorrected marker current. The size of the current correction is therefore a necessary reported diagnostic.

The transverse current is represented as linear in time between source endpoints. The propagating Fourier modes are then integrated analytically for that specified source representation by an exponential time-differencing update. The work integral $\int J \cdot E\, dt$ is evaluated consistently with the same representation. “Exact” in this method refers to the chosen stepwise source law and spectral update. It does not eliminate spatial discretization, source interpolation error or domain effects.

The zero Fourier mode requires separate treatment. More generally, a strictly periodic electric field has zero volume-integrated divergence, so an isolated nonzero net charge cannot be represented in a periodic cell without an explicit mean-charge convention or compensating construction. The nonzero-mode formula above does not resolve that issue. The zero-mode and background convention must accompany any future identification of this diagnostic with the nonzero-charge family in Section 6.

7.3 What the archived numbers establish

Table 1 reports the representative weak run with $N=36$, $L=8$, $M=160$ and $s_B=0.03$. These are archived measurements, not new Maxwell simulations performed for this article. The reference implementation normalizes each residual to its corresponding field or source scale. [Z6]

Table 1. Representative weak-branch numerical diagnostics.

Quantity	Archived value	Interpretation
Maximum continuity residual	5.5465×10^{-14}	Finite-step represented-source continuity
Maximum electric Gauss residual	4.2739×10^{-15}	Represented divergence constraint
Maximum magnetic divergence residual	8.4443×10^{-16}	Magnetic constraint diagnostic
Relative energy-balance residual	1.4604×10^{-14}	Field change plus analytic source work
Maximum imaginary-current leakage	2.1879×10^{-16}	Real-field representation control
Mean relative current correction	0.00449365	Approximately 0.4494 percent
Maximum relative current correction	0.0118416	Approximately 1.1842 percent
Maximum normalized marker speed	0.301334	Speed in the declared candidate units

The constraints and energy ledger are preserved near floating-point precision for this represented problem. Across the weak run family, the largest continuity and energy-balance residuals remain about 9.22×10^{-14} and 4.97×10^{-14} respectively. This is substantial evidence that the repaired representation behaves as intended. It does not establish an equally small error in the physical electron model or even in every computed field probe.

The distinction is visible in the refinement controls. Table 2 reports relative differences of the archived field-probe vectors between runs, rather than errors against a known exact physical solution.

Table 2. Probe sensitivity and retained controls.

Comparison	Relative difference	Assessment
Weak time steps 80 to 160	0.0040153	About 0.402 percent
Weak time steps 160 to 320	0.0043540	About 0.435 percent
Weak time steps 320 to 640	0.0017694	About 0.177 percent; finest contraction
Weak spatial grid 28 to 36	0.0666386	About 6.66 percent
Weak spatial grid 36 to 44	0.0041126	About 0.411 percent
Equal spacing with box enlarged from 8 to 10	0.0746413	About 7.46 percent; material box sensitivity

Comparison	Relative difference	Assessment
Strong time steps 80 to 160	0.2518321	About 25.2 percent
Strong time steps 160 to 320	0.2901322	About 29.0 percent
Strong time steps 320 to 640	0.2403936	About 24.0 percent; convergence failure retained

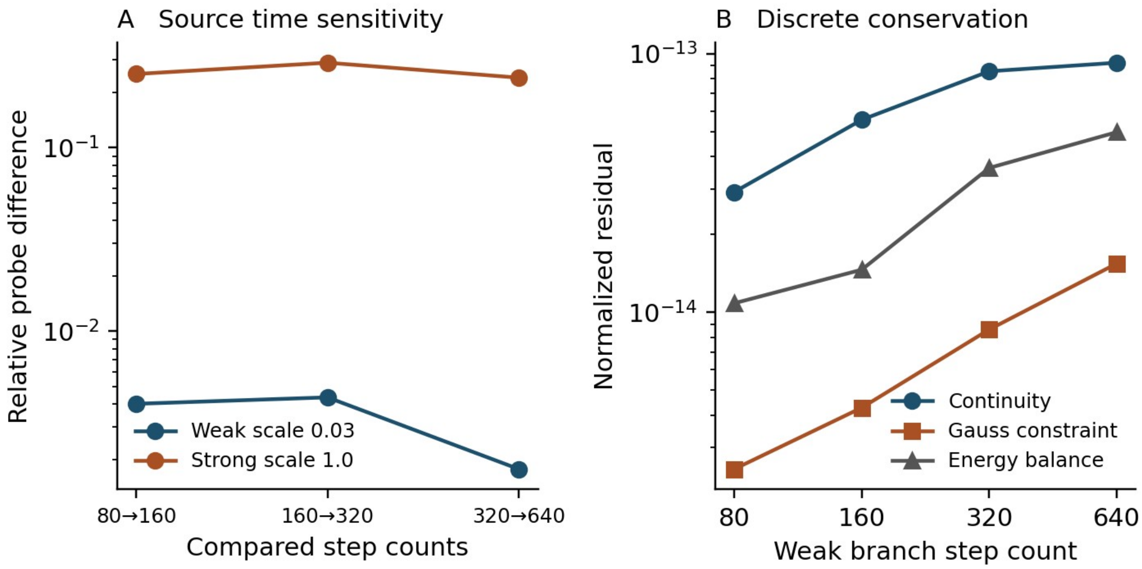

Figure 3. Archived G1 diagnostics replotted for this article. A contrasts weak and strong source-time probe differences. B shows weak-branch constraint and energy residuals. Small discrete conservation residuals coexist with larger probe sensitivity; these are different tests.

The finest weak time comparison contracts by a factor of approximately 0.406 relative to the preceding comparison, but the coarser differences are not monotonic. The results therefore do not warrant a blanket claim of demonstrated second-order convergence. Likewise, the approximately 7.46 percent response to an enlarged periodic box remains a practical uncertainty even though the weak branch passed its archived acceptance criteria.

The accepted mean-current-correction gate is a mean correction below three percent; it replaced an earlier relative-span diagnostic that failed. This change of metric belongs to the numerical history and should remain visible. A revised gate can be justified for a representation test, but it does not make the old negative result disappear. The strong branch is particularly instructive: very small constraint residuals can coexist with poor probe convergence because exact enforcement of a discrete identity is not a test of sufficient source-time resolution.

7.4 Reproducibility and physical scope

The canonical G1 record reports a prior deterministic replay of the representative weak run, agreeing with archived scalar metrics to a maximum absolute difference of approximately 5.03×10^{-17}. That is historical replay evidence. For the present article, all ten entries in the handoff checksum ledger were verified, the archived tables were reprocessed and the figures were regenerated. The Maxwell evolution itself was not rerun. [Z6]

The distributed v0.4 reference imports a helper named test_g1_exact_dynamic_maxwell_v0_3.py from an external v0.3 directory. That helper is not included in the v0.4 handoff supplied with this article. Historical provenance records its recovery, but the present supplement does not manufacture or substitute its contents. The reference also contains fixed working paths. A standalone replay therefore requires the recovered dependency bundle and deliberate path configuration before execution. This limitation concerns the completeness of this executable handoff, not the existence of the archived simulation.

G1 demonstrates a controlled Maxwell calculation for prescribed geometry and source motion. It does not evolve the spontaneous formation of the entire knot, obtain the source motion from its own field stress, establish radiation-free longevity in open space, or extract an electron scattering amplitude. Those would be different computational problems with additional equations and boundary conditions. The existing G1 branch supplies a tested part of the machinery needed for them.

8 From internal phase clocks to charge transport

8.1 Unit conversion is exact

A field model can contain several angular quantities: phase cadence, winding-coordinate speed, rotation of a local frame and motion of a charge source. They must be named before numerical values are compared. Let the G1 clock be

$$\tau=\frac{t}{t_*},\, t_*=\frac{L_*}{c}.$$

For a physical phase $\phi(t)$, the dimensionless phase rate is exactly

$$\hat{\omega}=\frac{d\phi}{d\tau}=\omega t_*.$$

With the declared local ruler $L_*=R_{out,L1}=\Gamma_L/(4\pi^2)$, where Γ_L denotes the project's local reference length, the current clock dictionary gives $\hat{\omega}_{Local}=1/(2\pi)$ and $\hat{\omega}_{L1}=2$. This conversion solves a time-unit problem. The symbol Γ_L here is a length reference and is distinct from the numerical driving coefficient Γ in Section 7. [Z7]

8.2 The source transport law is an additional relation

Suppose a source sheet is parameterized by $X(\xi,\tau)$ and carries a phase

$$\Phi(\xi,\tau)=k_\xi \xi-\hat{\omega}\tau+\Phi_0.$$

A constant-phase point has $d\xi/d\tau=\hat{\omega}/k_\xi$. Only if the physical charge transport is locked to that phase point can one write

$$\Omega=\frac{\hat{\omega}}{k_\xi},\, v_t=\Omega\,\partial_\xi X,\, K=\sigma_s\Omega\,\partial_\xi X.$$

Here σ_s is a surface charge density and K the corresponding surface current in the declared units. Motion of the sheet itself must be included separately when necessary. The phase-locking statement is constitutive: a moving interference pattern need not carry charge at its phase speed. [Z7]

8.3 Binary depth has its own interpretation

The six-cycle parameter also produces a conditional binary-depth coordinate

$$x_{21}=\frac{\beta_6}{1-\beta_6}=12.83670064502909\ldots,\, g_{21}=2^{x_{21}}=7315.29660248809\ldots.$$

The current model interprets x_{21} as a depth coordinate, with g_{21} the multiplicative factor under the stated immediate-parent and TimeSink assumptions. The earlier additive absolute-rate interpretation is superseded. The depth and the construction count in Appendix A share upstream information; they are not independent empirical confirmations. Even a valid internal rate factor needs an observer map before it becomes a laboratory frequency. [Z7, Z10]

8.4 Normalized cycles and raw cycle counts

In a common observation window of one Local tick, the stated L1 rate produces a raw count 4π. A candidate L2 assignment gives $4\pi g_{21}$ under its additional rate-ownership assumptions. Expressing either count in Local-cycle-equivalent units multiplies it by the inverse of its declared rate ratio, so its normalized value is one. This is an exact unit conversion, not physical attenuation, destruction of cycles or a prediction that an instrument resolving every native cycle would register one event. [Z7]

The present reference length is $\Gamma_L = 8.86 \times 10^{-22}$ m, with reference cadence $\omega_L = 2\pi c / \Gamma_L$. Its role is a reference-wave ruler and clock. It does not make that cadence an electron orbit or turn the reference length into a measured electron radius. Stating these owners prevents an otherwise correct normalization identity from being counted as an additional dynamical success.

9 Electron positron symmetry and proton reconstruction

The electron–positron face rule exchanges the designated electric and magnetic sectors:

$$C_Z : \left(E_{out}, B_{in}\right)_{e^-} \leftrightarrow \left(B_{out}, E_{in}\right)_{e^+}.$$

On the specified two-state set, the operation is an involution, $C_Z^2 = I$, and exchanges the states without a fixed point. The archived finite checker passed all eight face-symmetry checks. The positron allocation follows from the electron allocation and the shared exchange rule; it is not an unrelated third allocation premise. [Z8]

This finite symmetry result is narrower than a complete physical charge-conjugation model. It does not by itself derive opposite laboratory electric charges, equal masses, spinor transformation laws or annihilation amplitudes. In particular, a magnetic-primary outer sector in an internal face description must not be reinterpreted as an observable magnetic monopole. That would require a map to operational electric and magnetic fields that the two-state permutation does not provide.

Proton reconstruction uses a different operation: inside-out radial reordering, including the reassignment of old L4 to the new L1 role while preserving the identities and capacities of the underlying sectors. It must not be conflated with the electron–positron face exchange. Nor should obsolete absolute-rate vectors be restored merely because the layer names change. The geometry supplies a reconstruction route; the complete inversion dynamics and the calibrated proton observables require their corresponding calculations. [Z11]

The project's descriptions of outward electron transport as a fountain or inverse TimeSink, and inward behavior in its positive-particle constructions, are also frame-owned statements. They are not interchangeable with the direction of a circulating electric current or with a laboratory E/B label. Keeping those meanings separate makes it possible to examine their relationships without using a single visual metaphor as an equation of motion.

10 How the geometry becomes an electron observable

10.1 The ordered four-sector electric readout

Zero Theory already specifies an observer-facing electric readout in its Zero frame. The path order is L4 to L3 to L2 to L1 to the observer. An inner electric contribution encounters a magnetic coefficient before the next electric contribution is added. The working throughput rule is

$$T(E,B)=\frac{E^2}{E+B}.$$

This is a structural model rule. Its E and B arguments are frame-owned readout coefficients, not automatically the SI field magnitudes, radial thicknesses or charges used elsewhere. With the specified coefficients, the recursion is

$$R_{43}=T\left(0.25,0.75(4\pi-1)\right), R_{32}=T\left(R_{43}+\pi,\pi\right),$$

$$R_{21}=T\left(R_{32}+0.75(4\pi-2),0.25\right), Q_E^{(0)}=R_{21}+0.75.$$

The successive transmitted values are approximately 0.007002975342886, 1.576050507435436 and 9.257238179974825, giving $Q_E^{(0)}=10.007238179974825$. The final L1 electric contribution is added directly because no further magnetic coefficient lies in front of it on the stated path. Stopping after the first transmission or replacing the recursion with a simultaneous sum computes a different quantity. [Z12]

This is a complete four-sector structural readout at its declared level. The remaining task is to connect that level to a calibrated experiment. The value is dimensionless; it is not charge in coulombs, electron mass or the magnetic g factor. In particular, the throughput rule must not be silently substituted for the Maxwell transfer dynamics or for the damping recurrence in Section 5.

10.2 Charge and scattering

The normalized source family fixes how charge is assigned within the model, while a physical charge measurement requires the total source and its coupling to an external probe. A useful geometrical test would calculate the electromagnetic response as momentum transfer varies. For an experimentally meaningful comparison, the probe kinematics, frame, orientation distribution and normalization must be fixed before the result is evaluated.

“Pointlike” in a scattering description is an operational statement about resolved structure in the measured channel and range of momentum transfer. It does not require every internal explanatory variable to have zero extent. Conversely, the existence of a compact internal geometry does not guarantee pointlike scattering. Zero Theory’s route needs a target-independent form-factor or response calculation, not an identification of the smallest internal length with the experimental resolution scale. [Z9]

10.3 Spin and magnetic moment

A field can carry angular momentum without being a rigid rotating body. A candidate electromagnetic contribution is

$$J_{EM}=\int r\times\left(\epsilon_0 E\times B\right)d^3x,$$

evaluated with the complete common-frame field and supplemented by any required source contribution. For a localized stationary current, the corresponding magnetic-moment integral is $\mu=1/2\int r\times J\,d^3x$. Specifying these standard candidate functionals does not evaluate them for the knot. A satisfactory calculation must determine their values and their detector coupling from the same state.

The project’s nonrigid route avoids treating every internal phase contour as a piece of rigid matter. Its rigid comparison is nevertheless useful: with $I=C_I m r^2$ and fixed angular momentum S, the equatorial speed scales as $v=S/\left(C_I m r\right)$. Shrinking a rigid object increases that speed. Thus small size alone does not repair a rigid classical spin construction. The control does not rule out every nonrigid field model; it identifies an inadequate argument. [Z9]

The induction-owned half-angle law now establishes an exact 4-pi recurrence of the complete oriented and layer-labeled scalar state. Equivalently, its half-angle factor changes sign after 2-pi and returns after 4-pi:

$$\exp\left(i\frac{2\pi}{2}\right) = -1, \qquad \exp\left(i\frac{4\pi}{2}\right) = +1$$

This is a necessary double-cover-like kinematic signature and is stronger than a visual analogy with a closed curve. It is not yet a complete derivation of electron spin one half. The model must still lift the scalar state to a unique physical rotational state, evaluate the total field-plus-source angular momentum and show |S| = ℏ/2 without inserting that value, and derive exchange statistics and the two-outcome Stern-Gerlach measurement rule. A global sign is not observable in isolation; the model must specify the interference or detector coupling through which the sign difference is read. The same principle applies to magnetic resonance: a Penning-trap frequency ratio is not a direct movie of literal internal rotation.

For the idealized cyclotron and spin frequencies entering the operational comparison,

$$\nu_a = \nu_s - \nu_c, \frac{g}{2} = \frac{\nu_s}{\nu_c} = 1 + \frac{\nu_a}{\nu_c}.$$

The Zero Theory operational map includes a normalized cyclotron reference and its stability control. The remaining physical calculation must connect the complete internal response to the measured channels, including the trap interpretation. As a stringent experimental benchmark, Fan and colleagues reported $g/2 = 1.00115965218059(13)$ in 2023, with a relative uncertainty of 0.13 parts per trillion. That measurement constrains a proposed response model; it is not evidence for a particular toroidal geometry. It is cited here as a precision benchmark, not as a claim about the newest available measurement. [Z9; E6]

10.3.1 Clean half-action result and claim boundary

The spin result used in this manuscript belongs only to the attached L1 helical mode. It is not obtained from archived prescribed-source transport settings or from the earlier static complete-field angular-momentum diagnostic. Those calculations address a different numerical problem and are excluded from the present one-half inference.

For a helical path whose axial-to-tangential advance ratio is q, the same-mode one-turn clock and the same-mode angular-momentum-to-energy ratio give eta-turn = omega-turn Jz/Uattached = 1/(1+q squared). At the equal-component gate q = 1, eta-turn is exactly one half. Unequal controls q = 0.5 and q = 2 give 0.8 and 0.2, so the program does not impose one half as a universal output.

The result is independent of radius, propagation speed and uniform field amplitude because those quantities cancel inside the same helical mode. With the explicitly conditional bridge Uattached = hbar times omega-turn, it gives Jz = plus or minus hbar/2. Promotion from this mode-owned result to total electron spin remains open until the bound L1 contribution is identified without double counting inside a complete source-plus-field L1-L4 ledger.

10.4 Mass as a response involving matter

The model's mass architecture treats a material detector as a participant in the interaction. An electron state and a detector state interact, the detector changes, and an observer reads that calibrated change. This is more specific than assigning a number to an isolated sector and calling it a measured mass. At the declared relative-coefficient level, the common factorized law is

$$q_e = 1, q_p = (4\pi - 1)(4\pi)^2, K_{ij} = \kappa q_i q_j.$$

The coefficients therefore satisfy $K_{ep}^2 = K_{ee} K_{pp}$. The q_i in this expression are relative response weights, not electric charges. The relation links electron–electron, electron–proton and proton–proton coefficients without fitting three independent values. It is an exact consequence of the factorization premise. It does not yet determine the absolute interaction scale κ or convert the coefficients into an SI inertial mass. [Z9]

This route suggests an appropriate order of calculation: derive a common interaction law, evaluate the detector response, calibrate the measurement operation, and then compare with a mass or Compton measurement. Entering the measured electron energy at the first step and recovering it at the last would be calibration, not a new prediction.

The separate L2 expression $R_{e,L2}=6\,v_2$ remains a symbolic channel candidate. Its former absolute numerical calibration depended on the superseded additive-rate interpretation and is not restored here. A channel index, the ordered Zero-frame electric readout and a calibrated complete mass response are three different constructions, even when they share the same electron architecture. [Z7, Z12]

11 Input output comparison with recent geometric electron research

Toroidal and zitterbewegung models form a family of related but physically different proposals. Visual similarity is not a scientific comparison. The relevant comparison is an input-output ledger: which field or particle structure is assumed, which measured electron quantities are inserted or used to fit parameters, which equations are solved, and which reported results remain independent. The publications below are a selected, source-checked set from 2025 and 2026 rather than an exhaustive priority survey.

Table 3. Input-output ledger for selected recent electron models and the present construction.

Work	Structural or theoretical inputs	Measured or fitted inputs	Independent outputs and comparison
dos Santos and Fleury 2025 [E1]	A toroidal electromagnetic ansatz with free amplitude, major radius, minor radius and frequency; a finite torus mask; Maxwell consistency conditions.	Electron charge e, spin hbar/2 and magnetic moment including the leading anomalous term are imposed as parameter constraints.	Returns a phase velocity 2c, Compton-scale geometry, a Schwinger-scale amplitude and energy near 0.8 m_e c^2. These are valuable consistency outputs, but the fitted observables are not independent predictions.
dos Santos January 2026 [E2]	Toroidal fields with a stress-balance and electromagnetic-topology construction.	Experimental charge, magnetic moment and self-energy are used in reverse determination of model parameters.	Reports a more tightly calibrated toroidal electron. Numerical recovery of the calibration quantities is not an independent test; free perturbative stability remains a separate question.
dos Santos March 2026 [E3]	The preceding toroidal electron plus a specified relativistic helical transformation and selected probe geometry.	The rest-electron scale and the calibrated toroidal parameters are inherited from the earlier construction.	Recovers relativistic energy and momentum in the chosen boost and obtains a Bessel-type response. The result is more phenomenological than the present audit but is not a parameter-free derivation of spin one half.
Hestenes 2025 [E4]	The Dirac equation, spacetime algebra, a Dirac spinor and lightlike toroidal zitterbewegung.	The Dirac equation already contains m_e, e and hbar, and its spinor representation already carries the spinorial rotation structure.	Provides a detailed physical interpretation of the electron clock, local observables and gyromagnetism. It does not derive the one-half coefficient from a restricted Maxwell-field input set.
Sanctuary 2026 [E5]	A bivector and quaternion-like angular construction with internal angular vectors and toroidal projection.	Quantum angular-momentum normalization is part of the algebraic physical interpretation rather than extracted from the present Maxwell helix ledger.	Offers a distinct algebraic route to zitterbewegung and internal motion. Similar toroidal imagery does not establish identical assumptions, fields or independent outputs.
Zero Theory version 2.2	A four-layer field genealogy; an attached equal-component L1 helix; Maxwell-normalized E and cB; the field momentum relation; and a one-turn clock owned by the same helical mode.	No e, m_e, magnetic moment, g factor, alpha, Compton radius, field amplitude or target hbar/2 is supplied. The later unit bridge U_attached = hbar omega_turn introduces hbar but not the coefficient one half.	Derives eta_turn = 1/(1+q^2), hence exactly 1/2 at q = 1, with unequal controls 0.8 and 0.2. The result is mode-owned and conditional; confinement and non-overlapping promotion to the complete L1-L4 electron remain open.

The distinction is explicit in the 2025 electromagnetic model [E1]. It begins with four free quantities, E0, R0, r0 and omega. Charge is then constrained by Q_RMS = e; the magnetic-moment expression is matched to the Bohr magneton with the leading Schwinger correction; and the angular-momentum expression is required to equal hbar/2. The resulting field amplitude, radii, frequency and approximate energy are nontrivial consistency outputs.

The fitted e, magnetic moment and hbar/2, however, cannot simultaneously be listed as independent predictions. The same accounting applies to the reverse-calibrated continuation [E2].

The Hestenes construction [E4] has a different scientific purpose. It begins with the Dirac equation and its spinor degrees of freedom, including m_e, e and hbar, and develops a realist electron-clock and gyromagnetic interpretation. It therefore supplies a stronger connection to established spinor dynamics than Zero Theory presently has, but it is not a blind extraction of the one-half coefficient from Maxwell geometry. The relativistic toroidal continuation [E3] and the bivector construction [E5] likewise answer different questions and should be compared at the level of inherited inputs rather than imagery.

The present Zero Theory result deliberately has a narrower input budget. The calculation does not receive the electron charge, mass, magnetic moment, g factor, fine-structure constant, Compton radius, absolute field amplitude or the target hbar/2. It derives eta_turn = 1/(1+q^2) and obtains eta_turn = 1/2 from the equal-component gate q = 1. The later bridge U_attached = hbar omega_turn supplies the unit of action and yields the conditional J_z = plus or minus hbar/2; it does not supply the coefficient one half. Accordingly, the independent output is the dimensionless coefficient and its cancellation of radius, speed and amplitude, not a derivation of hbar itself.

A second boundary is equally important. Maxwell transversality and |E| = c|B| produce an equal orthogonal pair and therefore a 45-degree bisector in the normalized E-cB component plane. Identifying that bisector with the axial and tangential advances of the attached L1 helix is a declared Zero Theory physical map, not a theorem of Maxwell electrodynamics alone. The current literature ruling is therefore cautious: among the closely related models examined here, none derives the same exact one-half coefficient from the same restricted input set. This is not yet an exhaustive priority claim. Promotion from the L1 mode to total electron spin still requires confinement, a non-overlapping source-plus-field angular-momentum ledger and free dynamics.

12 A programme of discriminating calculations

The present results make the next calculations concrete. The first is a quantitative capture law. It should use a stated physical field profile to evaluate energy transferred per encounter into the mirror sectors, retain a complete energy ledger and predict the dependence on curvature and phase mismatch. A transfer coefficient chosen afterward to reproduce a desired construction count would not test the proposed mechanism.

The second is a constitutive phase-to-current law. The present revision derives the geometric half-angle transport inside Zero Theory from two distinct ingredients: Maxwell-normalized transverse equality and the model-specific frozen, symmetric L1-L4 frame assignment. The next calculation should independently test whether free interface-stress and field evolution preserve that transport while deriving the relation between phase, current and source motion. The mismatch between the structural transport candidate and the archived source rate remains a useful discriminating case. A successful common law must explain why the archived candidate is an appropriate realization, or specify a newly justified candidate and test it as a new branch.

The third is a self-consistent stability calculation. Field and source degrees of freedom should respond to their shared stress rather than following an imposed orientation path. The calculation should include perturbations of radial shape, phase allocation, source distribution and pair symmetry. Open-boundary or sufficiently controlled domain studies are needed to distinguish storage from radiation and periodic-image effects. This task extends the reduced stability results; it does not relabel them as results they never claimed to be.

The fourth is a detector-level electron calculation. Charge, angular momentum, magnetic response and momentum-transfer dependence should be evaluated from the same model state and observer convention. The physical electron targets used for comparison should be withheld from parameter selection wherever an independent prediction is claimed. The normalized detector coefficient identity and the operational frequency ratio already supply useful consistency tests, but each needs its dynamical input.

Finally, reproducibility should connect the geometry, source generator, helper dependencies, solver, units, tolerances and output tables in one executable specification. A change in any of these defines a changed computational question. Negative controls should remain available alongside the accepted branch so that a new success is measured against the same failure modes.

13 Conclusion

Zero Theory presently supplies a connected four-sector electron architecture, an audited complete-field energy ledger for a prescribed numerical problem, a corrected one-direction helical flux construction, an exact conditional half-angle recurrence for the oriented L1-L4 state, and an exact one-half action ratio for the one-turn clock of the equal-component attached L1 helix. The half-action result does not use archived source-motion defaults, a chosen radius, an absolute field amplitude, or a fitted target. With the explicitly conditional same-mode quantum bridge Uattached = hbar times omega-turn, it gives Jz = plus or minus hbar/2. The manuscript additionally identifies a limited observer-charge mechanism: phase-locked electric and magnetic layer directions can leave a persistent outward electric projection at the L1 boundary, which an external observer reads operationally as charge-like sign and response. Neither the Coulomb magnitude nor the elementary charge is derived here. The remaining spin gate is to identify the attached mode as a non-overlapping part of the confined complete knot and close the full source-plus-field angular-momentum ledger. Magnetic moment and the g factor remain downstream tests.

14 Reconstruction results and revised physical scope

14.1 Complete four layer energy stability

The energy question is owned by the complete four-sector field, not by four independently isolated layer energies. If E = sum_i E_i and B = sum_i B_i, the field energy includes all inter-layer cross terms.

$$\mathrm{U_4(t) = ½ \int\Omega\ [|\Sigma_i E_i|^2 + |\Sigma_i B_i|^2]\ dV}$$

Consequently, summing four separately evaluated energies would change the physical question. The legacy simulator instead assembles the four-layer sources in one three-dimensional periodic computational domain, evolves the common Maxwell field, and evaluates the complete-field energy. Its finite-step balance is tested against the integrated source work.

$$\mathrm{[U_4(t_1) - U_4(t_0)] + \int_{t_0}^{t_1}\int\Omega\ J\cdot E\ dV\ dt = R\_E}$$

In the archived N = 44 run, $U_4(t_0)$ = 0.03393423494735366, $U_4(t_1)$ = 0.03393423608699910, and the integrated source work is $-1.139645443390772\times10^{-9}$ in solver units. The relative closure residual is $8.466587086926782\times10^{-17}$. The associated marker normal-current leak diagnostic is $6.245004513516506\times10^{-17}$. These values establish numerical energy accounting for the declared four-layer prescribed-source problem. With the complete four-layer system taken as the electron boundary, no net energy escape is observed in this audited ledger. A separate open-boundary calculation is still required to quantify radiation into unbounded external space; that is a different question from conservation within the four-layer system.

Ruling. The demonstrated complete-field energy closure is a numerical property of a prescribed source history and of the consistent field and source-work update. It does not promote any prescribed source-motion setting to a uniquely derived electron rate. That historical diagnostic is kept separate from the clean half-action result.

14.2 Geometry driven shape response

To test shape without prescribing a time-dependent deformation, the fixed-axis aspect coordinate was completed into a two-component area-preserving quadrupole. The amplitude A and orientation phi_def are represented by

$$\mathrm{q\_c = A\ \cos(2\varphi\_def), \qquad q\_s = A\ \sin(2\varphi\_def).}$$

The source compiler, four-layer pairing, and weak generalized-force operator were evaluated on the resulting family without treating archived source-motion defaults as reconstruction targets. In the v0.9 audit, nonzero angular shape forces appeared away from symmetry axes, with opposite signs at mirror-related orientations and zero sampled angular circulation. In the expanded v0.10 audit, all 42 states passed the 10^-12 continuity gate; the largest relative residual was 3.020095703009663x10^-14. At fixed sampled orientations, the radial shape force retained one sign from A = 0.02 to A = 0.60, and no sampled amplitude root was bracketed.

Direct result. The reduced four-layer geometry produces an orientation-dependent, nonzero generalized response in shape space. Within this prescribed-source diagnostic, deformation is therefore not merely a verbal addition: the geometry supplies a calculable tendency to change shape.

Limits. A generalized force is not a velocity and the scan is static. The result does not require the physical electron to deform at every instant, does not prove that deformation grows without bound, and does not establish a rotating bulge or a closed deformation orbit. It also does not overturn the observed absence of net energy escape from the complete four-layer ledger. A static or moving stable state would require an evolution law, inertia or mobility, and the missing frame-transport axis or SO(3) connection. Deformation is consequently an allowed and geometry-supported outcome, not a precondition for the already demonstrated numerical energy closure.

14.3 What is solved and what remains open

The manuscript now uses three labels consistently. Established means directly reproduced by the supplied calculation. Conditional means an exact consequence of declared model premises. Open means that an independent physical derivation or converged dynamical calculation is still missing.

Item	Status	Present meaning
Four-layer energy ledger	Established numerically	Complete-field energy, cross terms, and source work close for the prescribed periodic-domain run.
45-degree L1 helix	Conditional	Follows when tangential and axial advances are equal; it is not the incidence angle.
Directed helical flux	Established for the stipulated mode	The linear field average vanishes, while $E\times B \propto \cos^2\varphi$ retains one direction.
720-degree recurrence	Conditional and executable	The oriented, labeled half-angle state returns after 4π; the unoriented control returns after 2π.
Physical spin magnitude	Open	No independent SI action closure yet maps the same state to the relevant electron spin observable.
Charge and g factor	Separate downstream branch	They require a probe-coupling and magnetic-moment calculation; they are not prerequisites for the present kinematic audit.
Exact helical half action	Conditional and executable	For q = 1, the same-mode turn clock gives eta-turn = 1/2; unequal controls return 0.8 and 0.2.
Observer-facing charge appearance	Conditional mechanism	Phase-locked layer vectors can leave a persistent outward electric projection; Coulomb magnitude and e are not derived.

Question	Current result	Claim boundary
Four-layer energy accounting	Passed for the declared common-field numerical problem	Not yet an open-boundary proof of a self-sustained electron

Finite-step charge continuity	Passed in the audited prescribed-source branches	Does not derive the physical source law
Shape response	Nonzero and orientation dependent in the reduced quadrupole family	No time evolution, period, or compulsory deformation established
Static shape equilibrium	No simultaneous sampled root in the audited family	Does not imply energy escape and does not rule out other closures
Charge, rest energy, spin, moment, scattering	Candidate functionals and readout roles are specified	Not yet co-evaluated from one self-consistent state
Scalar spin recurrence	Exact first labelled-state return at 4-pi	Does not uniquely select a spatial axis
Observer-facing electric projection	Mechanism stated from phase-locked layer vectors and ordered boundary readout	Does not yet predict Coulomb normalization, elementary charge or scattering

14.4 Comparison discipline and the missing common state

The comparative review changes the emphasis but not the architecture. Zero Theory's distinctive addition is the constrained two-wave, four-sector organization with separate genealogy and electromagnetic pairing, conditional construction arithmetic, an ordered readout, and an audited common-field simulation. Other recent geometric electron models provide calculations that this article still lacks: explicit analytic field integrals, local stress-balance constructions, Dirac-spinor dynamics, internally generated toroidal projection, or specified relativistic form factors. In several of those works, measured electron quantities also enter parameter selection; such recovered quantities are reconstructions rather than independent predictions. The same input-output accounting is applied here.

The decisive remaining task is one common self-consistent state. From that same state and one observer map, the programme must evaluate charge, total rest-energy candidate, angular momentum, magnetic moment, and at least one momentum-transfer or scattering response. Until that calculation is supplied, the article presents a constrained architecture with verified conditional and numerical components, not a completed physical derivation of the electron.

14.5 Executable completion programme

1. Preserve the v1.0 geometry and the complete-field energy ledger as fixed baselines.
2. Derive the source and frame-transport law from the phase and layer dynamics instead of preserving arbitrary numerical defaults.
3. Evolve the geometry and sources together; record scale, quadrupole amplitude, orientation, topology, layer order, charge closure, source work, field energy, and boundary flux.
4. Classify a run as energetically stable when the complete four-layer energy balance closes within a declared convergent tolerance. Deformation may be absent, bounded, periodic, or quasiperiodic; it is not itself a failure criterion.
5. Classify a closed moving-shape state only after bounded amplitude, nonzero winding where claimed, topology preservation, and geometric return are demonstrated under refinement.
6. Complete the field-plus-source angular-momentum ledger, derive the transport law and SI map, and then evaluate charge, angular momentum, magnetic response, rest-energy candidate, and scattering from that same state before claiming an electron observable.

Revised conclusion. The reconstruction does not overturn the four-layer numerical energy-stability result. It narrows its meaning and strengthens its audit trail. The same investigation finds a geometry-driven shape response in the reduced quadrupole family. Separately, the attached equal-component L1 helix gives an exact mode-owned one-half action ratio without importing archived source-motion settings. The next advance is to obtain a common dynamical state whose complete angular-momentum ledger, conservation laws, shape history, units, and electron observables can be evaluated together.

15 Historical v0.14 surface-force control

Layer ownership. For the electron, L1 is the observer-facing outer shell and L4 is the hidden symmetric partner of the complete outer Maxwell pair. The positron is the declared mirror role reversal. The present calculation evaluates the electron-side L1 transaction and does not manufacture a positron by relabelling the electron's L4 partner markers.

15.1 Normalized post attachment geometry

The project gate tan theta equals ds z divided by ds t gives theta equal to 45 degrees when the local axial and tangential advances are equal. After capture, the surface-following propagation direction is written as follows.

$$\hat{k} = \cos(\theta)\ \hat{t} + \sin(\theta)\ \hat{z}, \quad \theta = 45°$$

The incident electric amplitude is normalized to one. Both independent transverse polarizations are evaluated with B external equal to k hat cross E external. No physical amplitude, frequency, wavelength, phase lag, damping, capture efficiency, interaction duration, measured spin, magnetic moment or electron mass is inserted.

15.2 Force power and torque ledger

For each L1 source marker, the audit evaluates the external Lorentz force, instantaneous work rate and torque about the L1 centre.

$$F = q(Eext + v \times Bext), \quad P = \Sigma\ q\ v \cdot Eext, \quad \tau = \Sigma\ r \times F$$

Polarization	Active L1 torque per A	Full numerical torque per A	Power per A	Cycle mean torque per A
Radial	0	0	0	-2.32×10^{-19}
Helical transverse	+0.1767766953	−0.5303300859	+0.1272792206	$+5.90 \times 10^{-19}$

Interpretation of the numerical total. The full prescribed L1 coefficient includes −0.7071067811865467 from the v0.3 OUTER BOUNDARY sheet. That sheet is a periodic-domain neutralizer rather than a predicted physical electron surface charge. Its contribution is retained as a numerical control and the full-ledger value is not promoted as the physical electron torque.

15.3 Historical result and corrected scope

The marker calculation reproduces the analytic sin theta cos phase coefficients to relative error below 1.1 times 10 to the minus 15. The 45-degree gate supplies the expected one over square root of two projection. It is the equal-component point, not the angle of maximum torque.

Across sixteen uniformly spaced phases, the v0.14 helical-polarization mean axial Lorentz coefficient was 5.897220616504012 times 10 to the minus 19 and the mean power coefficient was 3.362608126677088 times 10 to the minus 18. These numerical zeros remain valid for that field-linear marker response. Stage v0.15 shows that they are not the cycle average of the directed energy and momentum flux of the composed traveling mode.

$$\Delta Jz = \int \tau z(t)\ dt$$

Historical-control ruling. The v0.14 calculation established a nonzero instantaneous marker-force channel but asked the wrong averaging question for propagation direction. Its demand for a phase lag merely to prevent directional cancellation is superseded by the corrected flux calculation in Section 16.

16 Corrected axial incidence and helical L1 composition

Clarified geometry. For the electron, L1 remains the observer-facing outer shell and L4 its hidden symmetric partner. The external wave incident on L1 propagates along the surface normal, perpendicular to the ring plane. L1 already supplies the azimuthal circulation. The positron is the declared mirror role reversal; this section evaluates the electron-side L1 composition.

16.1 The 45-degree resultant is a helix

Let ds t denote the tangential advance around L1 and ds z the axial advance carried by the attached external wave. When ds z equals ds t, the resultant path tangent has equal orthogonal components. The incoming ray is normal to the L1 plane; 45 degrees is the angle of the composed attached path, not the incidence angle.

$$\hat{\mathrm{h}} = (\hat{\mathrm{t}} + \hat{\mathrm{z}})/\sqrt{2}, \quad \mathrm{r}(\varphi) = (\mathrm{R}\,\cos\varphi,\ \mathrm{R}\,\sin\varphi,\ \mathrm{R}\varphi)$$

One full circulation advances by 2 pi R along the axis. The path length is 2 pi square root of two R, while curvature and torsion are both 1 divided by 2R for the positive-handed branch. If the total propagation speed is c, each component is c divided by square root of two. Assigning c independently to both components would incorrectly give a resultant speed of square root of two c.

16.2 Phase and directed energy flux

The oscillating field amplitude is proportional to cosine of phase, so its linear cycle mean is zero. A traveling electromagnetic wave reverses E and B together. Consequently the Poynting vector E cross B is proportional to the square of cosine and does not reverse the propagation direction.

$$\langle \cos\varphi \rangle = 0, \quad \langle \cos^2\varphi \rangle = 1/2, \quad \mathrm{S} \parallel \hat{\mathrm{h}}$$

Quantity	Executed value	Interpretation
Resultant angle	45 degrees	Equal axial and tangential advances
Tangent and axial shares	0.7071067811865475 each	Total speed remains c
Mean linear factor	$-2.7755575615628914 \times 10^{-17}$	Numerical zero
Mean Poynting factor	0.5	Positive directed cycle mean
Negative-flux samples	0 of 65536	No directional reversal
Path-length relative error	$1.2255713797366717 \times 10^{-8}$	Passes 5×10^{-8} tolerance

16.3 Conditional angular-momentum content

For an attached wave packet of energy U attached, the momentum magnitude is U attached divided by c. The equal-component helix assigns one over square root of two of that momentum to the azimuthal direction. Its signed angular momentum about the L1 axis is therefore the following.

$$\mathrm{Jz}/\mathrm{Uattached} = \pm\mathrm{R}/(\sqrt{2}\ \mathrm{c}), \quad \mathrm{Jz}/\mathrm{Pz} = \pm\mathrm{R}$$

The sign is the handedness. At the explicit numerical control R equals U attached equals c equals one, J z is 0.7071067811865475. This number is a normalization check; it is not a measured electron spin, not hbar divided by two, and not an independently selected physical radius or energy.

16.4 Ruling and remaining knot

Ruling. The directional-cancellation knot is removed. Under the clarified geometry, the axial external wave and L1 circulation form a one-direction 45-degree helical energy and momentum flux. No added phase lag is required merely to keep that propagation direction from reversing.

The remaining knot is no longer whether the 45-degree helix can generate a one-half action ratio; Section 16.5 shows that it can. The open question is ownership within the complete electron. The model must show that the attached helical energy remains bound, identify its contribution without double counting the common L1-L4 field, and close the source-plus-field angular-momentum ledger. Only then may the conditional hbar/2 result be promoted from the L1 helical mode to the complete electron.

16.5 Natural turn clock and the exact one-half action ratio

A clock is a repeated physical event, not an interchangeable numerical rate. For the attached helix, the relevant event is one complete azimuthal turn of the same energy-flow path used to calculate Jz. Let q denote axial advance divided by tangential advance. Speed normalization fixes the tangential and axial components rather than assigning c to both.

$$v = c/\sqrt{(1+q^2)}, \qquad vz = qc/\sqrt{(1+q^2)}$$

The path length of one turn is 2 pi R sqrt(1+q squared). Its period and angular turn frequency are therefore the following.

$$Tturn = 2\pi R\sqrt{(1+q^2)}/c, \qquad \omega turn = c/[R\sqrt{(1+q^2)}]$$

The same helical momentum decomposition gives Jz/Uattached = R/[c sqrt(1+q squared)]. Multiplication cancels the radius and propagation speed. The general turn-clock action ratio depends only on the pitch ratio.

$$\eta turn = \omega turn \; Jz/Uattached = 1/(1+q^2)$$

At the equal-component gate q = 1, the resultant angle is 45 degrees and the turn-clock action ratio is exactly one half. The executable v0.16 audit scans q = 0.5, 1, and 2 while independently varying R and c. The equal-component cases return 0.5 with zero floating-point deviation in the scan; the unequal controls return 0.8 and 0.2. The program therefore does not encode one half as a universal answer.

The quantum bridge is conditional but direct. If one quantum of this same bound mode has energy Uattached = hbar times omega-turn, then Jz = ±hbar/2, with the sign set by handedness. No absolute radius, energy amplitude, electron mass, electric charge, or g factor is used in this cancellation.

$$Uattached = \hbar\omega turn \qquad \Rightarrow \qquad Jz = \pm\hbar/2$$

Clock-ownership firewall. The omega in this inference counts the same one-turn recurrence whose U and J appear in the ratio. A six-cell material coordinate, a layer-frame slip rate, a prescribed source-transport rate, and the natural frequency of the complete knot are different clocks unless a separate bridge proves them equal. If n independent field-phase cycles occur during one geometric turn, their phase frequency is n times omega-turn and cannot silently replace the turn clock in this argument.

Ruling. The equal-component helical geometry derives an exact one-half dimensionless action for its own natural turn clock. Under the same-mode quantum-energy bridge it yields a conditional hbar/2 angular momentum. Promotion to the complete electron requires a bound-mode identification and a non-overlapping L1-L4 plus source ledger, not a backward fit of frequency.

17 L1 observer and blind L1 L4 field frame readout

Observer ruling. The external observer does not read the hidden layers separately. For the electron, L1 is the observer-facing shell and L4 is its hidden symmetric partner. The internal layers may determine the complete state, but the observable spin interpretation must be carried to the detector through an explicit L1 response. The internal angular-momentum ledger and the external readout are therefore related but are not interchangeable definitions.

17.1 Field defined local frames

When the electric and magnetic identities are frozen to their respective layer geometries, their directions define a right-handed local frame on each layer. The L1 observer reconstructs F1 from E1 and B1 and reconstructs F4 from E4 and B4 only for the relative comparison. The signed angle chi14 is the rotation from the L4 field frame to the L1 field frame about their common propagation normal. The L1 electromagnetic phase phi1 must be extracted independently from the L1 mode rather than inferred from chi14.

$$\chi_{14} = \mathrm{Angle}[F_1(E_1,B_1),\ F_4(E_4,B_4)]$$

17.2 Maxwell basis and the frozen-pair bridge

The 45-degree element must first be separated from the layer rule. In a locally plane, vacuum-like electromagnetic mode, Maxwell transversality gives E perpendicular to B and both vectors are perpendicular to the propagation direction. Their dimensions differ, so the comparison is made with the normalized magnetic vector cB. The vacuum relation $|E| = c|B|$ then makes E and cB an equal-length orthogonal pair. The diagonal of that transverse right-angle sector is consequently 45 degrees from either component. This 45-degree bisector follows from equal normalized components; it is not fitted from the measured electron spin, the electron g factor, or a desired 4π recurrence.

$$E \cdot B = 0, \quad |E| = c|B| \quad \Rightarrow \quad \arctan(|cB|/|E|) = 45^\circ$$

Maxwell theory supplies the orthogonality and normalized equality, but it does not by itself name L1 and L4 or attach a moving frame to either layer. That bridge is supplied by the Zero Theory geometry. The electric and magnetic directions are frozen to the two symmetric layer frames, and the equal 45-degree division is transported once as the relative orientation of the L1-L4 pair. Therefore a 90-degree advance of the L1 electromagnetic phase corresponds to a 45-degree change of the pairwise frame angle. Additivity then gives a 90-degree pairwise slip after 180 degrees of phase advance.

17.3 Relative-angle ownership and avoidance of double counting

Let $\theta 1$ and $\theta 4$ denote the orientations of the two layer frames relative to any chosen common reference. The observable used here is not either absolute angle separately. It is the single pairwise quantity $\chi 14 = \theta 1 - \theta 4$. Changing the common reference can change $\theta 1$ and $\theta 4$ while leaving $\chi 14$ unchanged. Consequently the two 45-degree field shares must not be counted again as two independent 45-degree layer rotations. That would double the intended relative slip.

$$\Delta\chi_{14} = \Delta\theta_1 - \Delta\theta_4 = \tfrac{1}{2}\Delta\varphi_1$$

A symmetric common-frame representation makes the bookkeeping explicit: $\Delta\theta 1 = +\Delta\varphi 1/4$ and $\Delta\theta 4 = -\Delta\varphi 1/4$. At 90 degrees of phase these are +22.5 and −22.5 degrees, whose difference is 45 degrees. At 180 degrees they are +45 and −45 degrees, whose difference is 90 degrees. An equally valid L4-fixed representation uses $\Delta\theta 1 = \Delta\varphi 1/2$ and $\Delta\theta 4 = 0$; it produces the same $\chi 14$. These are coordinate descriptions of one relative rotation, not different physical predictions.

L1 phase advance $\Delta\varphi 1$	Symmetric $\Delta\theta 1$	Symmetric $\Delta\theta 4$	Relative slip $\Delta\chi 14$
0°	0°	0°	0°
90°	+22.5°	−22.5°	45°
180°	+45°	−45°	90°
360°	+90°	−90°	180°
720°	+180°	−180°	360°

The final row expresses oriented-frame recurrence: a full 360-degree return of the relative L1-L4 frame requires 720 degrees of L1 phase. This is the model's spinorial kinematic signature. It establishes the half-angle transformation law, but it does not by itself assign the absolute angular-momentum magnitude $\hbar/2$; that later calculation still requires the physical energy, radius, and complete L1-L4 angular-momentum ledger.

17.4 Independent blind readout

The numerical readout is retained as an independent test of the derivation. It fits relative frame angle against independently extracted L1 phase with a free slope and intercept. The values one half, 90 degrees, 4π, $\hbar/2$ and the electron g factor are forbidden as fit constraints. A layer-separated free-slip run that returns a stable slope near one half would show that the dynamics preserve the geometric rule. A different stable slope would falsify or delimit the frozen symmetric-transport assumption rather than being hidden by the analysis.

$$\chi_{14} = a\varphi_1 + b + \varepsilon$$

Check	Executed result	Scientific meaning
Half-slope software fixture	0.49999999999999998	Analyzer recovery only
Arbitrary-slope negative control	0.36999999999999998	Shows one half is not forced
Target slope used in fit	False	Fit is numerically blind
Layer-separated G1 history	Not present	Scientific fit remains pending

17.5 Present result and next gate

Established within the declared model. Maxwell-normalized equality fixes the transverse 45-degree bisector, while the frozen symmetric L1-L4 assignment converts it into the pairwise law $\Delta\chi 14 = \Delta\varphi 1/2$ without importing the measured electron spin. The observer map is explicit and executable. The analyzer demonstrably recovers different slopes and does not encode one half as its answer. The 720-degree oriented-frame return is therefore an exact consequence of the stated field geometry and relative-angle bookkeeping.

Not yet established dynamically. The preserved G1 snapshots contain combined total-field probes rather than separate time-resolved L1 and L4 fields, and the common source frame does not supply a free relative-slip degree of freedom. The existing archive therefore cannot test whether a self-consistent Maxwell-interface evolution preserves the derived half-angle relation under perturbation. This missing run limits independent validation; it is no longer the logical source of the coefficient.

Next scientific question. Is the attached 45-degree L1 helical mode a confined, non-overlapping part of the complete L1-L4 electron state, so that its exact one-half turn-clock contribution survives the total source-plus-field angular-momentum ledger? A dynamically free, layer-separated evolution must then test whether the same turn clock and half-angle readout persist under perturbation while four-layer energy closes. The g factor remains downstream of magnetic moment and is not this gate.

18 Consolidated evidence and executable package map

The electron branch is distributed as two deliberately separate executable packages. The geometry package owns the four-layer knot, prescribed-source Maxwell calculations, energy closure, helical-flux construction, frame readout and historical controls. The clean spin package owns only the helical turn-clock action audit. Removing the retired complete-field spin audit from that package prevents a prescribed solver history from being mistaken for an input to the exact one-half result.

The geometry package contains conditional constructions and prescribed-source numerical experiments; it is not a self-consistent free-particle solution. The clean spin package proves the exact one-half turn-clock action ratio for the equal-component attached helix and includes unequal-component controls. Reproducing that package establishes a mode-owned geometric action ratio, not yet the total spin of a stable electron eigenmode.

Recommended current wording: the supplied electron branch contains a conditional labeled-state 4-pi recurrence, a corrected helical-flux construction, an exact one-half turn-clock action ratio for the equal-component attached L1 mode, and a limited observer-facing mechanism for charge-like appearance from phase-locked layer vectors. With Uattached = hbar times omega-turn for that same mode, the conditional angular momentum is hbar/2. What remains open is promotion to the complete confined L1-L4 electron, Coulomb and SI charge calibration, magnetic moment, and the g factor.

Package	Scientific owner	Claim ceiling
Electron geometry v1.0-C10	Electron knot geometry and Maxwell audit	Prescribed-source geometry, ledgers, controls, and conditional frame rules
Spin extraction v0.17 clean	Standalone helical half-action audit	Exact eta-turn = 1/2 at q = 1 with unequal controls; no total-electron spin claim

Appendix A Conditional construction count

The construction count is obtained from the same terminal parameter used in the six-cycle calculation, together with a declared injection rule. Starting with $C=4\pi-1$ and $\beta_6=C/6-1$, define

$$x_{21}=\frac{\beta_6}{1-\beta_6}=\frac{C-6}{12-C}, b_{inj}=\frac{2(8\pi)}{8\pi-2}=\frac{8\pi}{4\pi-1}.$$

The effective injection depth and continuous active contribution are

$$m_{eff}=x_{21}\frac{\ln 2}{\ln b_{inj}}, N_{inj,cont}=2^{m_{eff}}.$$

The two seeds are then added, while the active contribution is rounded upward to an even integer according to the specified closure rule. Here ceil denotes the smallest integer greater than or equal to its argument:

$$N_{build,cont}=N_{inj,cont}+2, N_{closure}=2\,ceil(N_{inj,cont}/2)+2.$$

Table A1. Fresh arithmetic reproduction of the declared construction formulas.

Quantity	Value
β_6	0.92772843572652882564
x_{21}	12.83670064502909090719
b_{inj}	2.17291508863783790016
m_{eff}	11.46510902453660274343
$N_{inj,cont}$	2827.10357604298591797319
$N_{build,cont}$	2829.10357604298591797319
$N_{closure}$	2830
$N_{closure}-N_{build,cont}$	0.89642395701408202681

The arithmetic was recomputed for this article using 55-digit decimal arithmetic. No measured electron mass, Compton wavelength, magnetic anomaly or local electron-energy target enters the calculation. This verifies the conditional numerical chain, not the injection premise from microscopic dynamics. The final count is not a measured particle property and is not automatically a photon count. The shared use of β_6 and x_{21} must also be preserved when counting independent assumptions and successes. [Z10]

Appendix B Notation and dimensional ownership

Symbol	Meaning in this article
L_i	Phase sector of the complete wound field
C_i and $C = 4\pi - 1$	Continuous model capacities
N in Sections 3 and A	Recurrence or construction count as explicitly labeled
N in Section 7	Number of grid points along one coordinate
M	Number of source-time intervals
α	Uniform phase coordinate; not the fine-structure constant
a_Q	Charge-allocation parameter
q	Radial interface fraction when used for the 75/25 partition
q_e, q_p	Relative material-response weights; not electric charges
R and s	Curvature radius and transverse offset in the planar support comparison
$u(s)$	Support profile with the units required by the planar integral
Γ_L	Zero Theory local reference length
Γ	Fixed G1 driving coefficient
$\hat{\omega}$	Phase rate per solver time
Ω	Source-sheet coordinate transport rate
k_ξ	Phase winding per source coordinate
x_{21}, g_{21}	Conditional binary depth and its exponential factor
s_B	Numerical driving scale, distinct from transverse distance s

Appendix C Evidence and reproduction statement

The source register contains 30 complete current semantic records, their identifiers and transport routes, the R2C11 and R2C14 focused audits, and the original G1 v0.4 handoff. The supplement preserves archived tables, checksum verification and the scripts for arithmetic and figures. Later explicit corrections govern the interpretation of historical prose.

The available transport contains 14 of 21 source parts. This bounded register does not certify complete recovery of the entire project. Fresh checks comprise archive integrity, conditional arithmetic and replotting archived data. No new Maxwell replay or experimental validation is claimed; the helper dependency in Section 7.4 remains explicit. The article is a standalone research manuscript and does not automatically modify the canonical core.

References

Zero Theory source groups

[Z1] Emamifar, S. M. H. Zero Theory R2C15 current semantic records: wave-knot phase-sector ontology; four-layer capacity; wounded co-rotating saturation. The complete record identifiers and transport filenames are listed in the supplementary source register.

[Z2] Emamifar, S. M. H. Zero Theory current records: electron six-saturation selection; six-phase lattice; phase stiffness. Includes equal-cell assumptions and the common-rotation and all-to-all-synchronization negative controls.

[Z3] Emamifar, S. M. H. Zero Theory current records: wound-mirror geometry; L1 local-observer geometry; L1 E/B cross section; L1/L4 frozen Maxwell pairing; L2/L3 parity-time cancellation. Includes supersession of the isolated-L1 branch.

[Z4] Emamifar, S. M. H. *Electron Foundational Pillar Recovery and Curved-Wave Transfer Audit*. R2-C14, claim package R2-C14-CA01 v0.1, 12 September 2026. Source excerpt and its transport locator are supplied in the supplement.

[Z5] Emamifar, S. M. H. Zero Theory current records: electron net-charge source family; complete-field stress-energy ownership.

[Z6] Zero Theory Team B. *G1 Dynamic-Maxwell Handoff v0.4*. Reference solver, source generator, simulator, run summary, control metrics, Nyquist audit and checksum ledger. Read with the current G1 simulation and electron integration-checkpoint records, including the documented 17 August 2026 recovery and replay.

[Z7] Emamifar, S. M. H. Zero Theory current records: G1 solver-clock adapter; phase-to-source transport control; rate-normalization bridge; L1-to-L2 binary-depth coordinate; Local cadence closure; rebased local-reference-wave cadence. Current semantics retain the source-transport mismatch and supersede the additive absolute scaffold.

[Z8] Emamifar, S. M. H. *Electron–Positron Face Symmetry Audit*. R2-C11 v0.1. Preserved support source and finite face-exchange verification.

[Z9] Emamifar, S. M. H. Zero Theory current records: nonrigid spin and pointlike readout; Penning operational map; pairwise material-detector mass architecture; field-manifold microdynamics upgrade. Each record retains its own resolution scope.

[Z10] Emamifar, S. M. H. Zero Theory current records: 2830 construction derivation; target-input firewall; L1-to-L2 binary-depth coordinate. Arithmetic independently re-evaluated for this manuscript.

[Z11] Emamifar, S. M. H. Zero Theory current record: proton inversion topology. Inside-out radial reordering is distinct from electron–positron face exchange.

[Z12] Emamifar, S. M. H. Zero Theory current records: Zero-frame ordered electric readout; L2 six-channel readout. The ordered throughput calculation is retained as a dimensionless structural result; the superseded absolute L2 channel calibration is excluded.

External research and experimental benchmark

[E1] dos Santos, C. A. M. and Fleury, M. J. J. *A Simple Electromagnetic Model of the Electron*. arXiv:2510.22384, version 2, 28 October 2025. Preprint. Source; full text.

[E2] dos Santos, C. A. M. *A Self-Consistent Toroidal Model of the Electron: Electromagnetic Topology and QED Correspondence*. Author-posted preprint, 26 January 2026. Source.

[E3] dos Santos, C. A. M. *Toroidal Electron: The Master of Disguise under Relativistic Helical Transformation*. Author-posted preprint, 31 March 2026. Source.

[E4] Hestenes, D. *Gyromagnetics of the Electron Clock*. IEEE Access 13, 53772–53803, 2025. DOI: 10.1109/ACCESS.2025.3544654. Author manuscript.

[E5] Sanctuary, B. *The Zitterbewegung in the Bivector Standard Model*. Axioms 15(2), 116, 2026. DOI: 10.3390/axioms15020116. The source-checked author preprint was posted 9 December 2025; its record identifies the subsequent publication. Author preprint and publication record.

[E6] Fan, X., Myers, T. G., Sukra, B. A. D. and Gabrielse, G. *Measurement of the Electron Magnetic Moment*. Physical Review Letters 130, 071801, 2023. DOI: 10.1103/PhysRevLett.130.071801. Article.